

The equation of state of nuclear matter above saturation density from intermediate energy heavy-ion collisions

M. D. COZMA(*)

Department of Theoretical Physics, IFIN-HH - Reactorului 30, 077125 Măgurele/Bucharest, Romania

received 26 November 2024

Summary. — The dcQMD transport model has been used to study different aspects of the in-medium nucleon-nucleon interaction, in particular the equation of state of nuclear matter by comparing theoretical predictions for nucleonic (stopping, directed and elliptic flows) and pionic (charged multiplicity ratio) observables in heavy-ion collisions at intermediate impact energies to available experimental data measured by the FOPI and S π RIT Collaborations, respectively. These studies have demonstrated the feasibility of constraining the equation of state of both symmetric and asymmetric matter up to twice the saturation density with unprecedented accuracy. Precise values for the compressibility modulus of symmetric matter and slope of the symmetry energy were extracted from nucleonic flow data: $K_0 = 230_{-11}^{+9}$ MeV and $L = 63_{-13}^{+10}$ MeV at 68% CL. The study of charged pion spectral ratios has led to $L = 79.9 \pm 37.6$ MeV in full agreement with nucleonic observables. Perspectives on improving the accuracy of these results and probing higher densities with heavy-ion collisions are also discussed.

1. – Introduction

A realistic description of heavy-ion collision (HIC) dynamics at intermediate energies requires accurate knowledge of different aspects of the in-medium nucleon-nucleon interaction: in-medium elastic and inelastic scattering cross-sections, optical potentials and equation of state (EoS) of nuclear matter (NM). The last one, in particular its isovector component commonly known as symmetry energy (SE), represents a crucial ingredient for a proper understanding of structure of nuclei close to drip lines, supernova explosions and properties of neutron stars. It has become increasingly more important during the last decade, after the advent of multi-messenger astronomy which has opened the possibility of answering questions related to the nature of matter at densities far above saturation. Additionally, HIC constraints for EoS can be compared to *ab initio* calculations in an effort to better understand the robustness and accuracy of the latter far above saturation density.

Traditionally, these three aspects of the in-medium nucleon-nucleon interaction have been individually determined by a comparison of transport model predictions for well

(*) E-mail: dan.cozma@theory.nipne.ro

chosen observables to experimental data. This has been possible due to the existence of a hierarchy among in-medium effects: modification of cross-sections has the largest impact on observables, followed by momentum dependence of the interaction, while the effect of EoS is generally the smallest. This strategy has been successfully applied by Danielewicz *et al.*: in-medium cross-sections were fixed by describing nucleonic stopping observables, in particular rapidity distributions; the momentum dependence of the interaction was subsequently determined by a comparison to transverse momentum elliptic flow of protons in peripheral HIC [1]. Lastly, the EoS of isospin symmetric matter was extracted from the slope of directed flow at mid-rapidity and elliptic flow in mid-central collisions [2]. Alternatively, information on in-medium cross-sections and optical potentials from independent sources can be used, the EoS being determined from a comparison of predictions for a suitable observable to experiment, such as v_{2n} [3].

A special category of observables that present significant sensitivity to the EoS but exhibit reduced dependence on in-medium cross-sections and optical potentials have been devised. In particular, the ratio of reduced multiplicity of K^+ strange meson produced in Au+Au *vs.* C+C collisions was found to show sizable dependence on the compressibility modulus K_0 of isospin symmetric nuclear matter (SNM) which has allowed a qualitative only conclusion that the EoS and SNM is soft [4,5], due to rather large uncertainties of experimental data. To study the symmetry energy the neutron-to-proton or neutron-to-hydrogen elliptic flow ratios [6], charged pion [7] and K^+/K^0 multiplicity ratios have been proposed [8]. Investigations using particle production in the vicinity of the threshold have proven challenging: attempts to extract the stiffness of SE from the charged pion ratio has led to a series of contradictory results [9,10], while kaon production in HIC has failed to exhibit the same sensitivity to SE as for uniform infinite nuclear matter [11]. The study of SE using neutron-to-proton, neutron-to-hydrogen and neutron-to-charged particles elliptic flow ratios has been fruitful, providing some of the most accurate constraints for the slope parameter L of SE at saturation [12,13].

This contribution focuses on a summary of two recent studies that have made use of the dcQMD transport model to study the EoS of NM followed by a discussion of near future prospects. In the first one transport model predictions for stopping, directed and elliptic flow for nucleonic observables are compared to an extensive subset of FOPI experimental data leading to constraints for the EoS of both isospin symmetric and asymmetric nuclear matter (ANM) alongside information for in-medium modification of elastic nucleon-nucleon cross-sections and optical potentials [14]. The second study was devoted to extracting information on SE from more exclusive pion production observables close to threshold measured experimentally by the S π RIT Collaboration [15].

2. – Model details

The transport model of choice was dcQMD, see refs. [13,14] for details. The employed parametrization of the potential part of the EoS, inspired by a Hartree-Fock calculation using the Gogny interaction [16], reads

$$(1) \quad \frac{E}{N}(\rho, \delta) = A_u \frac{\rho(1 - \delta^2)}{4\rho_0} + A_t \frac{\rho(1 + \delta^2)}{4\rho_0} + \frac{B}{\sigma + 1} \frac{\rho^\sigma}{\rho_0^\sigma} (1 - x\delta^2) \\ + \frac{D}{3} \frac{\rho^2}{\rho_0^2} (1 - y\delta^2) + \frac{1}{\rho\rho_0} \sum_{\tau, \tau'} C_{\tau\tau'} \iint d^3\vec{p} d^3\vec{p}' \frac{f_\tau(\vec{r}, \vec{p}) f_{\tau'}(\vec{r}, \vec{p}')}{1 + (\vec{p} - \vec{p}')^2 / \Lambda^2}.$$

The density ρ and isospin asymmetry δ dependence can be adjusted by fixing the compressibility modulus K_0 of SNM, magnitude of symmetry energy close to 2/3 saturation density $S(0.1 \text{ fm}^{-3})$ and slope L of symmetry energy at ρ_0 . The extra freedom provided by the term proportional to D is fixed by requiring that $J_0 = -600 + 3.125 \cdot (K_0 - 165)$ [MeV] and $K_{sym} = -488 + 6.728 \cdot L$ [MeV]. The choice for the skewness parameter J_0 is justified *a posteriori* by comparing the slope of compressibility at crossing density ($\rho_c \approx 0.11 \text{ fm}^{-3}$) with the value extracted from studies of giant monopole resonances [17]. The correlation between L and K_{sym} is of secondary importance for flow observables since the maximum sensitivity to SE lies close to ρ_0 , see below. The last term accounts for momentum dependence of the interaction. It is fully specified by choosing values for the isoscalar effective mass (m^*), neutron-proton effective mass difference (Δm_{np}^*) and strength of the isoscalar optical potential at infinitely large momentum U_∞ .

The propagation under the influence of mean-field interaction is described using the following Hamiltonian, in one-to-one correspondence with eq. (1):

$$(2) \quad \langle H \rangle = \sum_i \sqrt{p_i^2 + m_i^2} + \sum_{i,j,j>i} \left[\frac{A_+}{2} + \tilde{\tau}_i \tilde{\tau}_j \frac{A_-}{2} \right] u_{ij} + \sum_i \frac{B}{\sigma + 1} [1 - x \tilde{\tau}_i \delta_i] u_i^\sigma \\ + \frac{D}{\eta + 1} [1 - y \tilde{\tau}_i \delta_i] u_i^\eta + \sum_{i,j,j>i} \left[C_+ + \tilde{\tau}_i \tilde{\tau}_j C_- \right] \frac{u_{ij}}{1 + (\vec{p}_i - \vec{p}_j)^2 / \Lambda^2} + \sum_{i,j,j>i} U_{ij}^{Coul},$$

where $\tilde{\tau}_i = -\tau_i / T_i$, $u_{ij} = \rho_{ij} / \rho_0$ is the partial relative interaction density of particles i and j with $u_i = \sum_{j \neq i} u_{ij}$. Here T_i and τ_i denote the isospin and isospin projection of particle i , respectively.

The collision term makes use of in-medium elastic and inelastic cross-sections. For the former the following expression can be derived in the same manner as in vacuum by replacing energy and momentum variables by in-medium single particle energy and kinetic momenta,

$$(3) \quad \frac{d\sigma}{d\Omega} = (2\pi)^4 \frac{m_1^* m_2^*}{k_i^* \sqrt{s_i^*}} |M_{fi}^{(med)}(\rho, \delta, \{\tau\})|^2 \frac{k_f^* m_1^* m_2^*}{\sqrt{s_f^*}}.$$

Effective masses in the expression above are determined using the equations of motion and thus depend on local properties of the medium. Kinetic momenta are the same as canonical ones since the Hamiltonian corresponding to eq. (1) does not include vector interactions. The in-medium transition amplitude $M_{fi}^{(med)}$ is assumed to be related to the one in vacuum by

$$(4) \quad |M_{fi}^{(med)}(\rho, \delta, \{\tau\})|^2 = \frac{1}{2} (|M_{fi}^{(vac)}(\tilde{s}_i)|^2 + |M_{fi}^{(vac)}(\tilde{s}_f)|^2) \\ \times \exp \left[(\alpha + \beta_1 \delta + \beta_2 (\tau_1 + \tau_2) \delta) \frac{\rho}{\rho_0} \right].$$

The exponential factor induces an *ad hoc* dependence on density, isospin asymmetry and splitting of nn and pp elastic cross-sections in ANM in addition to the one induced by effective masses in kinematic factors. Their strengths can be modified by adjusting the values of α , β_1 and β_2 parameters, respectively. The vacuum transition amplitude $M_{fi}^{(vac)}$

is evaluated at an invariant mass ($\tilde{s}_{i,f}$) that is above threshold by the same amount of energy as the in-medium one ($s_{i,f}^*$),

$$(5) \quad \sqrt{\tilde{s}_{i,f}} - 2m_N = \sqrt{s_{i,f}^*} - \sqrt{s_{th}^*} + U_{i,f} - U_{th},$$

leading to threshold shift effects. Here, s_{th}^* represents the in-medium invariant mass at threshold. A correction term depending on single particle potentials occurs due to the momentum dependence of the interaction. For further details the reader is referred to ref. [14]. Inelastic channels are treated in a similar fashion [18].

3. – Equation of state

The FOPI Collaboration has measured several nucleonic observables in HIC of impact energies in the range of 0.09 to 1.5 GeV/nucleon for system with various isospin content ranging from isospin symmetric CaCa to neutron rich AuAu. A fraction of the published database has been used to study in-medium elastic cross-sections, momentum dependence of optical potentials and the EoS of NM by comparing theoretical predictions of the dcQMD transport model to experimental data [14]. The list of observables includes: *varxz* for proton, deuteron and triton for 14 systems with impact energy in the range 0.15 to 1.0 GeV/nucleon [19]; rapidity-dependent directed flow for $Z = 1, 2$ fragments for NiNi, XeCsI and AuAu at impact energy 0.25 and 0.40 GeV/nucleon [20]; rapidity-dependent directed flow for p, d, $A = 3$ and α clusters, rapidity and transverse-momentum-dependent elliptic flow for p, d, t and α clusters for AuAu reactions at impact energies of 0.15, 0.25, 0.40, 0.60 and 0.80 GeV/nucleon [21].

Transverse-momentum-dependent directed flow data have not been included in this list since a strong contamination of theoretical proton spectra by heavier fragments has been observed. Experimental results for this observable are available only for a range of reduced rapidities (larger than 0.5), where contributions from the decay of spectators are expected to be important. Hence, a transport model without explicit clusters degrees of freedom is expected to be somewhat unreliable in this region. Consequently, comparison of model predictions for rapidity-dependent v_1 and v_2 is restricted to the mid-rapidity region ($|y/y_P| \leq 0.5$). A similar argument has been used to exclude experimental data for the two lowest impact energies available, 0.09 and 0.12 GeV/nucleon. For projectile energies of 1.0 GeV/nucleon and higher the impact of nucleonic resonances degrees of freedom on reaction dynamics becomes non-negligible. Constraining their interaction with the medium requires inclusion of pionic observables in the mix. Due to shortcomings in describing two-pion decay channels of resonances, the dcQMD is presently not suitable for a robust analysis in this impact energy region. Therefore, available experimental data for flow observables above 0.8 GeV/nucleon have also not been included. Only flows and stopping observables in central and mid-central collisions, respectively, have been considered.

Eight transport model parameters have been determined from a fit to the above list of experimental data. They control in-medium modification of elastic nucleon-nucleon cross-sections (α, β_1, β_2), momentum dependence of optical potentials ($m^*, U_\infty, \Delta m_{np}^*$) and the density dependence of the EoS (K_0, L), see sect. 2 for their definition. In-medium cross-sections receive additional contributions from effective masses, see eq. (3), which induce a temperature dependence besides the one on density and isospin asymmetry via the equations of motions that are used to determine them during system's evolution.

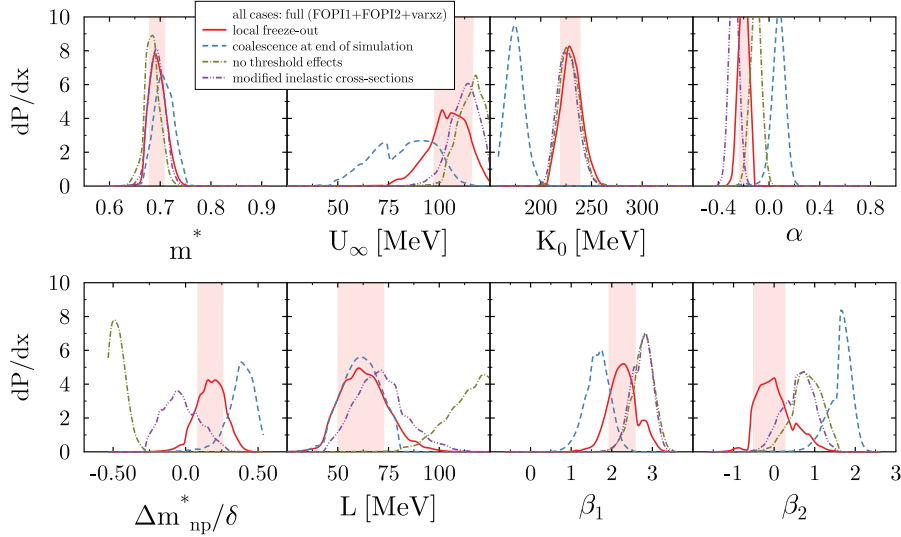


Fig. 1. – PDFs of model parameter values for four cases: coalescence applied at local freeze-out and end of simulations, threshold effects switched off and modification of inelastic NN cross-sections. For each parameter, the 68% confidence level interval is shown by a vertical shaded area. Three experimental data sets were used: stopping (varxz [19]), directed flow of $Z = 1, 2$ fragments (FOPI1 [20]) and directed and/or elliptic flow of $p, d, t, A = 3$ and α clusters (FOPI2 [21]). Figure taken from ref. [14].

Probability distribution functions (PDFs) for these parameters are determined using the maximum likelihood method. In the process, uncertainties of theoretical predictions are computed as the sum, in quadrature, of statistical and systematical uncertainties. The latter are determined by varying coalescence parameter cut-offs independently within a conservative range: $\delta r = 3.0\text{--}4.0$ fm and $\delta p = 0.2\text{--}0.3$ GeV/c.

In fig. 1 PDFs for the eight parameters are shown, the interval of variation being indicated by the range of abscissas. Four different scenarios are depicted: full model with observables determined by applying the coalescence afterburner at local freeze-out time or final time of the evolution $t = 150$ fm/c, threshold effects switched off and modified in-medium inelastic cross-sections. The first case represents the central result of the study, the additional ones show the impact of commonly used approaches in the literature. In particular, identifying clusters at freeze-out time has a significant impact on all three aspects of the in-medium effective nucleon interaction. Such a procedure, while having no impact on the dynamics of the reaction, corrects for spurious emission of nucleons from clusters that occurs in QMD-type models due to fluctuations, with significant impact on cluster multiplicities. Threshold effects are shown to have considerable impact on isovector observables. This holds true also for isoscalar ones if stopping observables are omitted from the fit. These are effective in fixing the density dependence of in-medium cross-sections, whose magnitude is correlated with the momentum dependence of optical potentials and the EoS. Lastly, the impact of nucleonic resonances degrees of freedom, via inelastic cross-sections in the collision term, is proven to be limited only to slight modification of in-medium elastic cross-sections which justifies the chosen upper limit of impact energy. Inclusion of isospin symmetric systems (CaCa, NiNi, RuRu - stopping;

NiNi - directed flow) is crucial in removing a degeneracy of in-medium effects on cross-sections that depend either on ρ or δ for AuAu reactions with impact on the extracted EoS, see ref. [14]. The constraints for density dependence of the EoS, at 68% CL, read: $K_0 = 230_{-11}^{+9}$ MeV and $L = 63_{-13}^{+10}$ MeV. Comparison of extracted EoS for SNM or ANM and pressure in neutron star matter ($\delta \approx 0.93$) with *ab initio* calculations, astrophysical observations and other nuclear physics experiments are provided in ref. [14].

A determination of the range of densities probed by the observables used to study the EoS is of uttermost importance. This can be achieved by a brute force calculation recognizing that observables are functionals of the EoS. To that end, the sensitivity can be defined as the functional derivative of the observable of interest with respect to the derivative of the EoS with respect to density, $(E/N)'$,

$$(6) \quad \frac{d\mathcal{O}}{d(E/N)'}(\tilde{\rho}) = \lim_{\varepsilon \rightarrow 0} \frac{1}{2\varepsilon} \left[\mathcal{O}\left(\frac{dE/N}{d\rho}(\rho) + \varepsilon\delta(\rho - \tilde{\rho})\right) - \mathcal{O}\left(\frac{dE/N}{d\rho}(\rho) - \varepsilon\delta(\rho - \tilde{\rho})\right) \right].$$

It induces a local modification of either L_0 (slope of the EoS of SNM) or L in the vicinity of target density $\tilde{\rho}$. This approach is computationally more advantageous compared to an equivalent definition using the functional derivative with respect to the EoS (E/N) which is more suitable when threshold effects generate the dominant sensitivity to EoS. In practice it is achieved by adding to the interaction Hamiltonian in eq. (2) the following terms:

$$(7) \quad \begin{aligned} \Delta\langle H_{L_0} \rangle &= \sum_{i=n,p} \frac{\varepsilon}{2} \left[\text{Erf}\left(\frac{\tilde{u}}{\eta}\right) - \text{Erf}\left(\frac{\tilde{u} - u_i}{\eta}\right) \right], \\ \Delta\langle H_L \rangle &= \sum_{i=n,p} \frac{\varepsilon}{2} \tilde{\tau}_i \delta_i \left[\text{Erf}\left(\frac{\tilde{u}}{\eta}\right) - \text{Erf}\left(\frac{\tilde{u} - u_i}{\eta}\right) \right] \end{aligned}$$

devised for the determination of sensitivity with respect to EoS of symmetric and asymmetric nuclear matter respectively at target reduced density \tilde{u} . The parameter η represents the width of Gaussian used to approximate the Dirac δ function appearing in eq. (6), with its value set to $\eta = 0.125$.

The sensitivity of proton collective flows in AuAu HICs to the EoS of SNM and ANM is presented in fig. 2, though similar results were obtained for all other light cluster species. The left panel shows the sensitivity of rapidity dependent directed flow $v_1(y)$ to L_0 for three different impact energies and two ranges of rapidities. Two ranges in densities, subsaturation and suprasaturation, show significant sensitivity with a region of reduced sensitivity in-between as a result of the existence of the saturation point. In the suprasaturation regime, a migration of the location of maximum sensitivity with increasing beam energy is observed. In particular, at 0.8 GeV/nucleon impact energy there is significant sensitivity close to twice saturation density and above. Clearly, by increasing beam energy the EoS of SNM at ever higher densities can be constrained using flow observables. A similar calculation for the sensitivity of transverse-momentum-dependent elliptic flow, $v_2(p_T)$, with respect to the slope L of SE is presented in the right panel of fig. 2. In this case the sensitivity reaches a maximum close to saturation, independent of the impact energy, and becomes insignificant above $1.5\rho_0$. Different observables, in particular particle production, may facilitate studying the SE in the vicinity of $2\rho_0$ and above.

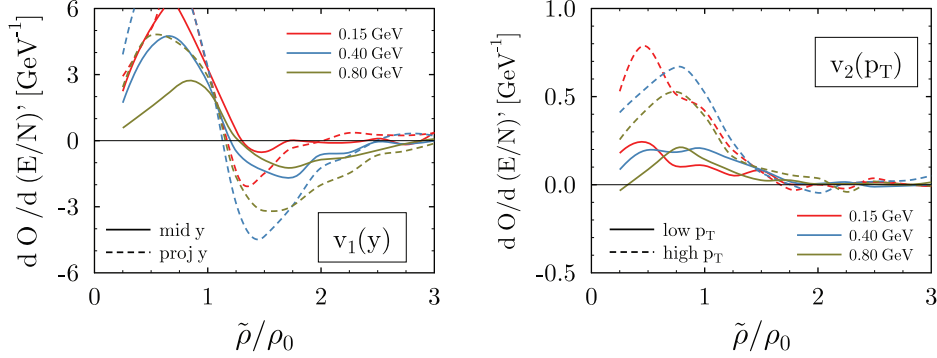


Fig. 2. – Sensitivity of rapidity-dependent directed flow $v_1(y)$ (left panel) and transverse-momentum-dependent elliptic flow $v_2(p_T)$ (right panel) of protons to the density dependence of EoS of SNM and ANM, respectively, as a function of density for mid-central ($0.25 < b_0 < 0.45$) AuAu collisions. In both panels color denotes impact energy of the projectile, while style of curves denotes ranges in rapidity or transverse momentum. Figures taken from ref. [14].

Turning to pion production, efforts to understand initial difficulties have led to the understanding of importance of threshold shift effects for particle production close to threshold. They lead to an enhancement of particle multiplicities as a result of more attractive potentials in the final state of individual two-body collisions as compared to the initial one [22]. In qualitative terms the biggest effect is the result of the momentum dependence of the interaction and change of momenta in inelastic collisions. The isospin asymmetry dependence of the interaction can play a similar role due to non-locality of elementary collisions coupled with charge exchange reactions. Such effects were shown to have a non-negligible impact on the charged pion ratio [23, 24] and are crucial for a thermodynamically consistent description of uniform nuclear matter using transport models [25]. A quantitative description also requires the knowledge of resonance [18, 26] and pion [27, 28] in-medium potentials.

A dedicated measurement of pion production close to threshold with the aim of studying the SE has been carried out by the S π RIT Collaboration. Experimental data for HICs of four Sn isotopes combinations have been gathered at a beam energy of 0.27 GeV/nucleon. Two of these, the neutron rich $^{132}\text{Sn}+^{124}\text{Sn}$ and neutron deficient $^{108}\text{Sn}+^{112}\text{Sn}$ central ($b \leq 3.0$ fm) HICs, have been used for a quantitative determination of the slope parameter L [15]. A precise determination was however hindered by a couple of aspects: the charged pion ratio shows significant sensitivity to Δm_{np}^* [18] and the dcQMD could only be compared to experimental data for large transverse momenta, $p_T \geq 0.2$ GeV/c. At lower momenta, non-resonant pion production becomes important, a channel that is not considered in the model, and a strong sensitivity to the in-medium $\Delta(1232)$ potential has also been demonstrated.

The dcQMD version employed in these pion studies relied on empirical in-medium elastic cross-sections [29] and isoscalar optical potential together with a slightly higher compressibility modulus $K_0 = 245.0$ MeV. These choices lead to a reasonable description of FOPI flow data [18], which is a prerequisite for a realistic description of HIC reactions. S and P waves pion optical potentials that allow a good description of pion spectra at low p_T have also been included [15]. The value of SE at two thirds saturation density was fixed to $S(0.1 \text{ fm}^{-3}) = 25.5$ MeV [30]. At this stage the only free parameters of the

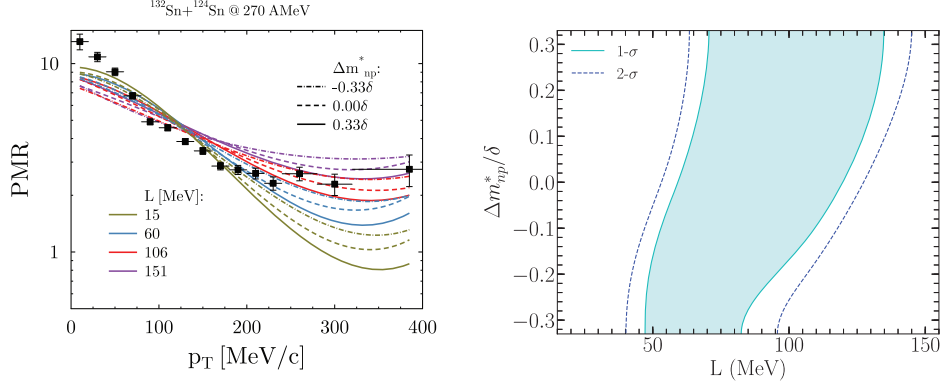


Fig. 3. – Left: theoretical predictions of the charged pion spectral ratio for 12 sets of values for $(L, \Delta m_{np}^*)$ compared to experimental data for the neutron rich $^{132}\text{Sn} + ^{124}\text{Sn}$ system. Right: 68 and 95% confidence level regions in $(L, \Delta m_{np}^*)$ parameter space extracted from a combined analysis of the charged pion spectral ratios for neutron rich $^{132}\text{Sn} + ^{124}\text{Sn}$ and neutron deficient $^{108}\text{Sn} + ^{112}\text{Sn}$ systems subject to $p_T \geq 0.2 \text{ GeV}/c$. Figures taken or adapted from ref. [15].

model are L and Δm_{np}^* . Simulations for 12 sets of values for them were performed, a comparison of theoretical predictions to experiment is shown in the left panel of fig. 3. A χ^2 -analysis of combined $^{132}\text{Sn} + ^{124}\text{Sn}$ and $^{108}\text{Sn} + ^{112}\text{Sn}$ data for the pion spectral ratio, subject to $p_T \geq 0.2 \text{ GeV}/c$, was employed to determine the region in parameter space compatible with experiment, see the right panel of fig. 3, leading to $L = 79.9 \pm 37.6 \text{ MeV}$ at 68% CL.

The sensitivity of pionic observables to SE as a function of density is determined in identical fashion as for nucleonic flows. Results for the single pion ratio in central AuAu collisions ($b \leq 2.0 \text{ fm}$) for three different impact energies (0.4, 0.8 and 1.2 GeV/nucleon) are shown in the left panel of fig. 4. The sensitivity peaks at deep subsaturation densities and monotonically decreases with increasing density, becoming negligible above $2\rho_0$. Clearly, using pion production the SE can be studied up to twice saturation density, provided accurate experimental data are available. Interestingly, with increasing beam energy, the pion ratio at high p_T becomes more sensitive, while compared to lower beam energies the sensitivity is reduced. However, the fraction of sensitivity above $1.5\rho_0$ remains fairly constant with increasing impact energy.

Consequently, a constraint for SE above saturation density can be extracted from experimental pion production data. For that the density dependence below saturation is fixed (SE with a slope at saturation L_1). From a comparison to experimental data, here the pion spectral ratio in $^{132}\text{Sn} + ^{124}\text{Sn}$ HICs with $p_T \geq 0.2 \text{ GeV}/c$, the density dependence above saturation is determined, encoded in a slope parameter at saturation L_2 . Varying the value L_1 a family of EoSs with slope L_2 above saturation are determined. Due to the anti-correlation of values for L_1 and L_2 they cross in a density region approximately given by $\rho_c/\rho_0 = 1.45 \pm 0.05$, see the right panel of fig. 4, leading to $S(1.45\rho_0) = 44 \pm 4 \text{ MeV}$. To make calculation more tractable the neutron-proton effective mass difference has been fixed, $\Delta m_{np}^* = -0.08\delta$. Precise knowledge of the symmetry energy below saturation, *e.g.*, $S(0.1 \text{ fm}^{-3}) = 25.5 \pm 1.0 \text{ MeV}$ [30], is crucial for the approach to be feasible.

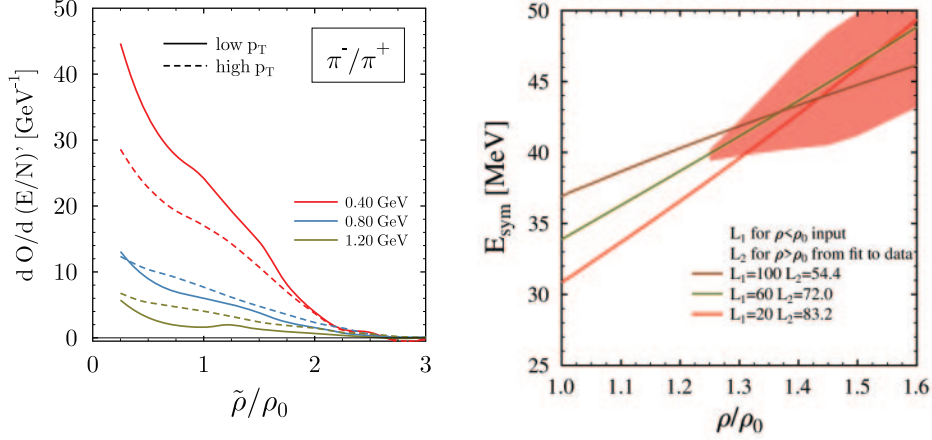


Fig. 4. – Left: sensitivity of the pion spectral ratio in central AuAu collisions ($b \leq 2.0$ fm) as a function of density for three beam energies. Values for low ($p_T \leq 0.2$ GeV/c) and high ($p_T \geq 0.4$ GeV/c) transverse momentum ranges are shown. Right: symmetry energy density dependence constraints above saturation, encoded by the slope parameter L_2 , are determined from comparison to experimental data (see text) after fixing the density dependence of SE below saturation (slope parameter L_1). The shaded area depicts the region enclosed by the envelope of the family of constrained EoS (only a limited range in L_1 was used to generate constraints for L_2).

4. – Perspectives

In the previous section it was shown that the charged pion ratio close to threshold provides the highest sensitivity to SE above saturation among the studied observables. A feasibility study proved the potential of constraining the magnitude of SE close to $1.5\rho_0$

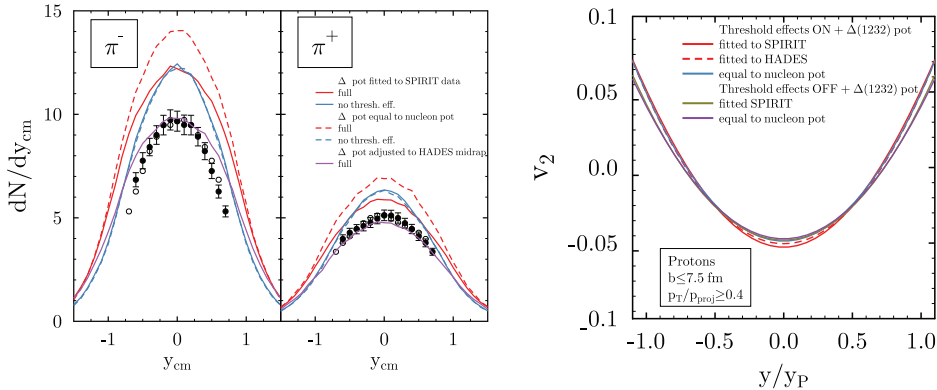


Fig. 5. – Left: predictions for rapidity spectra of charged pion produced in central AuAu at an impact energy of 1.23 GeV/nucleon. Results for different choice for the $\Delta(1232)$ potential are shown, with threshold effects included or not. HADES experimental data are shown as symbols [31]. Right: impact of the $\Delta(1232)$ potential on proton elliptic flow for AuAu collisions at 1.0 GeV/nucleon impact energy. Calculations including or excluding threshold effects are shown.

with an accuracy of about 4 MeV, provided the value of Δm_{np}^* is known. That shortcoming has been removed by a recent interpretation of FOPI stopping and flow data using the same transport model [14]. To increase accuracy of constraints the limitation of using only the high p_T region of pion spectra has to be lifted, making thus use of the more accurately measured data. To that end non-resonant pion production channels, which become increasingly more important towards threshold, have to be included in the transport model, an effort which is currently in progress. Additional experimental measurements of pion production close to threshold by the S π RIT (XeSn at 0.34 GeV/nucleon) and HADES (AuAu at 0.4, 0.6 and 0.8 GeV/nucleon) Collaborations have the potential to further increase the accuracy of results.

To access higher densities using nucleonic observables the robustness of the dcQMD transport model above 1.0 GeV/nucleon impact energy has to be improved. In this region $\Delta(1232)$ potentials begin to have a visible impact on nucleonic observables. For example, in AuAu collisions at 1.0 GeV/nucleon beam energy, changing these quantities modifies predictions for proton elliptic flow by 10%, see the right panel of fig. 5, which amounts to about half the sensitivity to the EoS of SNM. Fixing the $\Delta(1232)$ can be most accurately accomplished by studying pion production. In particular, rapidity spectra of charged pions show significant sensitivity to these potentials, see the left panel of fig. 5. Interestingly, a quantitative description of HADES data for pion multiplicities at mid-rapidity requires $\Delta(1232)$ potentials that are more repulsive than those extracted from a comparison of model predictions to S π RIT or FOPI data [18]. This underlines the relevance of extra production channels close to threshold. To also describe the rapidity dependence of spectra, additional channels, such as two pion decay of $N^*(1440)$ will have to be consistently accounted for, as they provide mechanisms for converting energetic pions into softer ones, leading to a narrowing of rapidity distributions, as required by HADES experimental data [31]. Potential for increasing knowledge of the EoS above saturation will also be provided by the near future campaigns of the ASYEOS and HADES Collaborations that aim at measuring neutron-to-proton flows ratios and light cluster flows, respectively, at several impact energies below 1.0 GeV/nucleon with improved accuracy.

* * *

The author acknowledges financial support from the Romanian Ministry of Education and Research through Contract No. PN 23 21 01 01/2024.

REFERENCES

- [1] DANIELEWICZ P., *Nucl. Phys. A*, **673** (2000) 375.
- [2] DANIELEWICZ P., LACEY R. and LYNCH W. G., *Science*, **298** (2002) 1592.
- [3] LE FÈVRE A., LEIFELS Y., REISDORF W., AICHELIN J. and HARTNACK CH., *Nucl. Phys. A*, **945** (2016) 112.
- [4] FUCHS C., FAESSLER A., ZABRODIN E. and ZHENG Y.-M., *Phys. Rev. Lett.*, **86** (2001) 1974.
- [5] HARTNACK CH., OESCHLER H. and AICHELIN J., *Phys. Rev. Lett.*, **96** (2006) 012302.
- [6] RUSSOTTO P. *et al.*, *Phys. Lett. B*, **697** (2011) 471.
- [7] LI B.-A., YONG G.-C. and ZUO W., *Phys. Rev. C*, **71** (2006) 014608.
- [8] STURM C. T. *et al.*, *Phys. Rev. Lett.*, **86** (2001) 39.
- [9] XIAO Z., LI B. A. and CHEN L. W., *Phys. Rev. Lett.*, **102** (2009) 062502.
- [10] HONG J. and DANIELEWICZ P., *Phys. Rev. C*, **90** (2014) 024605.

- [11] LOPEZ X. *et al.*, *Phys. Rev. C*, **75** (2007) 011901.
- [12] RUSSOTTO P. *et al.*, *Phys. Rev. C*, **94** (2016) 034608.
- [13] COZMA M. D., *Eur. Phys. J. A*, **54** (2018) 40.
- [14] COZMA M. D., arXiv:2407.16411 (2024).
- [15] ESTEE J. *et al.*, *Phys. Rev. Lett.*, **126** (2021) 162701.
- [16] DAS C. B., GUPTA S. D., GALE C. and LI B. A., *Phys. Rev. C*, **67** (2003) 034611.
- [17] KHAN E. and MARGUERON J., *Phys. Rev. Lett.*, **109** (2012) 092501.
- [18] COZMA M. D. and TSANG M. B., *Eur. Phys. J. A*, **57** (2021) 309.
- [19] REISDORF W. *et al.*, *Nucl. Phys. A*, **848** (2010) 366.
- [20] ANDRONIC A. *et al.*, *Phys. Rev. C*, **67** (2003) 034907.
- [21] REISDORF W. *et al.*, *Nucl. Phys. A*, **876** (2012) 1.
- [22] FERINI G., GAITANOS T., COLONNA M., DI TORO M. and WOLTER H. H., *Phys. Rev. Lett.*, **97** (206) 202301.
- [23] SONG T. and KO C. M., *Phys. Rev. C*, **91** (2015) 014901.
- [24] COZMA M. D., *Phys. Lett. B*, **753** (2016) 166.
- [25] ZHENG Z. and KO C. M., *Phys. Rev. C*, **97** (2018) 014610.
- [26] IKENO N. and ONO A., *Phys. Rev. C*, **108** (2023) 044601.
- [27] COZMA M. D., *Phys. Rev. C*, **95** (2017) 014601.
- [28] ZHENG Z. and KO C. M., *Phys. Rev. C*, **95** (2017) 064604.
- [29] LI Q., SHEN C., GUO C., WANG Y., LI Z., LUKASIK L. and TRAUTMANN W., *Phys. Rev. C*, **83** (2011) 044617.
- [30] BROWN B. A., *Phys. Rev. Lett.*, **111** (2013) 232502.
- [31] ADAMCZEWSKI-MUSCH J. *et al.*, *Eur. Phys. J. A*, **56** (2020) 259.